TÜBİTAK

Turk J Elec Eng & Comp Sci, Vol.20, No.5, 2012, © TÜBİTAK
doi:10.3906/elk-1009-751

Circuit model and parasitic parameter extraction of the spark plug in the ignition system

Quandi WANG, Yali ZHENG*, Jihui YU, Jin JIA
State Key Laboratory of Power Transmission Equipment & System Security and New Technology, Chongqing University, Chongqing, CO 400030, P.R. CHINA
e-mail: yaya9304@163.com

Received: 13.09.2010

Abstract

This paper presents a circuit model of the spark plug in the ignition system for conducted electromagnetic interference (EMI). Based on the spark plug's current discharge channel, the circuit model of the spark plug is established with the parasitic parameters and the air-gap model. The parasitic parameters of the spark plug are extracted with the finite element method, and the air-gap model of the spark plug is analyzed using the electric circuit principles and the air-discharge theory. The simulation and measurement results validate this model. Furthermore, this model confirms that the spark plug discharge is the main conducted EMI source in the ignition system based on simulation.

Key Words: *Circuit model, electromagnetic interference/compatibility, finite element method, parasitic parameters, spark plug, ignition system*

1. Introduction

More and more electronic devices have been introduced into modern automobiles. The problem caused by the electromagnetic interference (EMI) of electrical systems is therefore becoming increasingly serious [1]. EMI may cause failure or malfunction of the electrical devices and affect both the safety and reliability of automobiles [2,3], which has aroused great concern among automotive manufacturers and designers. International and local institutions have standardized the electromagnetic compatibility (EMC). For example, the International Special Committee on Radio Interference (CISPR) indicated EMI standards with specifications on the threshold of the automotive electromagnetic radiation for conducted EMI (from 150 kHz to 30 MHz) and radiated EMI (from 30 MHz to 1 GHz) [4,5].

Recently, simulation techniques have been widely used in predicting EMC, including the finite element method (FEM), the method of moments (MoM), the finite difference time domain (FDTD) method, and the transmission line method (TLM) [6-12]. These methods can help to identify automotive EMC-relevant problems in the very early design stage and avoid intensive costs in the redesign cycles of the automobile development

*Corresponding author: Circuit model and parasitic parameter extraction of the spark plug in the ignition system

process. On the other hand, the ignition noise caused during engine operation is the most powerful EMI source in the automobile. Many measurements and simulations have been carried out for the study of ignition system EMI. However, EMC tests, according to the international standards, are expensive and time-consuming. Moreover, in these experiments, it is difficult to analyze the spark plug discharge mechanism [13,14]. Fujiwara and Amemiya proposed a spark plug circuit model in [15], and they used a simplified structure of the spark plug to obtain parasitic parameters. This simplified model could easily lead to parameter errors. In [16], Wang used the diode instead of the spark plug in the circuit model. However, the diode can only simulate the spark plug correctly before the spark plug breaks down, not in the stages afterwards. Until now, researchers have not described the spark plug discharge characteristics in detail in one working cycle.

A circuit model of the spark plug for conducted EMI is proposed in this paper after analyzing its internal discharge channel. The model takes into account the parasitic parameters and the spark plug air-gap discharge characteristics. With the FEM in the field solver, it is more precise if the parasitic parameters are extracted based on the real structure of the spark plug. The air-gap is treated as nonlinear dynamic resistance in the circuit model. Therefore, the spark plug discharge characteristics can be described by the circuit model in detail both before and after breakdown. The whole process of the spark plug discharge is simulated using the model placed in the ignition system. The results obtained by the simulation and the measurement prove the efficiency of the model proposed in this paper. Finally, the conducted EMI of the ignition system is simulated. The simulated results are consistent with the measured results, and this indicates that the spark plug discharge is the main conducted EMI source in the ignition system.

2. The circuit model of the spark plug in the ignition system

In analyzing the spark plug discharge problem, the spark plug current discharge channel is an overriding factor. As current i shooting through the unshielded center electrode is the dominant ignition current, the discharge channel and the corresponding circuit model of the spark plug are shown below in Figure 1 [14].

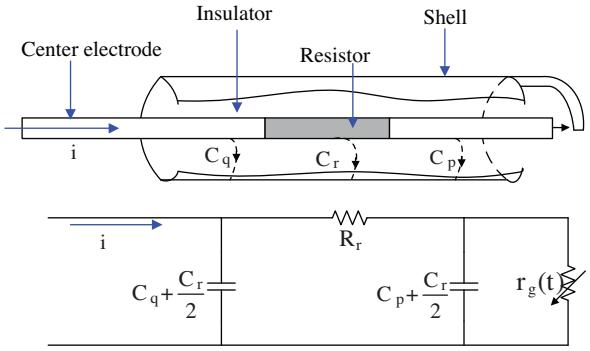

Figure 1. The discharge channel and circuit model of the spark plug.

In Figure 1, R_r is the series resistance and its value can be given by the manufacturers; r_g is the air-gap resistance of the spark plug; and C_q, C_r, and C_p are the parasitic capacitances between the center electrode and the shell.

Figure 2 shows the ignition system circuit model with the following simplifications: 1) the parasitic capacitances between the ignition system's modules are neglected and are finally added to the whole system; 2) the ignition coil circuit model is simplified here, which is expatiated in [17].

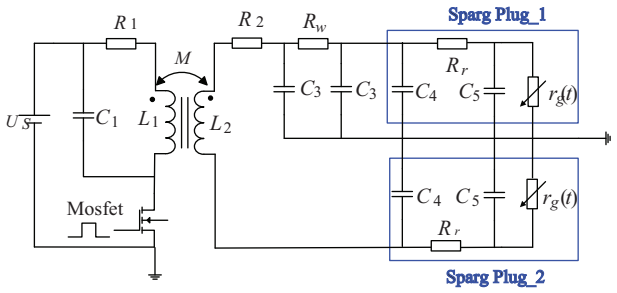

Figure 2. The circuit model of the ignition system.

In Figure 2, $C_4 = C_q + C_r/2$, $C_5 = C_p + C_r/2, C_3 = C_w/2$, U_s is the DC power supply, R_1 and R_2 are respectively the resistance of the primary and the secondary winding, L_1 and L_2 are respectively the inductance of the primary and the secondary winding, M is the coefficient of mutual inductance between the primary and the secondary winding, C_w is the parasitic capacitances between the high-voltage wire and the shell, and R_w is the resistance of the high-voltage wire.

3. The spark plug circuit model

3.1. Parasitic parameters extracted by the FEM

The inner electrical field of the spark plug can be taken as an electrostatic field for the analysis of the conducted EMI problem. Figure 3 shows the longitudinal section of the spark plug solution region. Parasitic parameters are extracted with the FEM.

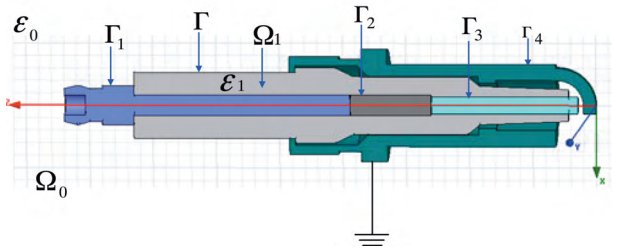

Figure 3. Longitudinal section of the spark plug solution region.

In Figure 3, $\Omega_1 \cup \Omega_0$ is the solution domain, Γ is the boundary of the insulation medium, Γ_i is the boundary of the ith conductor, and ε_1 and ε_0 are the permittivity of the insulation medium and the vacuum, respectively.

In the solution domain, the governing equations and the constitutive relation are:

$$\begin{cases} \nabla \times E = 0 \\ \nabla \cdot D = 0 \\ D = \varepsilon E \end{cases} . \tag{1}$$

When using the scalar potential $E = -\nabla\varphi$ and the FEM approach, Eq. (1) can be written as follows [18]:

$$\varphi \in \left\{ \varphi \in L^2, \nabla\varphi \in IL^2 \,|\varphi = f \ \text{ on } \ \Gamma_d \right\}. \tag{2}$$

That is:

$$\int_{\Omega} \varepsilon \nabla \varphi' \cdot \nabla \varphi d\Omega = \int_{\Omega_0} \varepsilon_0 \nabla \varphi' \cdot \nabla \varphi d\Omega + \int_{\Omega_1} \varepsilon_1 \nabla \varphi' \cdot \nabla \varphi d\Omega = 0$$

$$\forall \varphi' \in \left\{ \varphi \in L^2, \nabla \varphi \in IL^2 \,|\varphi = f \text{ on } \Gamma_d \right\}, \tag{3}$$

where Ω is the solution domain including Ω_0 and Ω_1, Γ_d is the Dirichlet boundary representing all Γ_i (i= 1, 2, 3, 4) boundaries, and f is the applied voltages on the conductors.

Eq. (3) leads to the following matrix equation:

$$[k]\,[\varphi] = 0, \tag{4}$$

where matrix $[k]$ is a function of the geometric parameters where the elements are connected with an interpolating function.

The parasitic parameters can be calculated by imposing 1 V onto the first conductor and 0 V onto the others in turn. For example, static potential $\varphi_j = 1$ V is applied to the jth conductor while grounding the others, and Eq. (4) is solved to obtain the potential distribution. Because the surface charge density on the conductor surface is $\sigma = \varepsilon E \cdot n$ ($\boldsymbol{n}$ is the unit vector of outward normal to the conductor surface), the electric charge of the ith conductor can be computed by:

$$Q_i = \varepsilon \oint_{\Gamma_i} E \cdot n d\Gamma_i. \tag{5}$$

Therefore, we can get the parasitical parameters from:

$$C_{ij} = \left. \frac{Q_i}{\varphi_j} \right|_{(\varphi_1, \cdots \varphi_{j-1}, \varphi_{j+1}, \cdots \varphi_m)=0, \varphi_j=1} \qquad (i \neq j). \tag{6}$$

3.2. Air-gap model of the spark plug

The spark plug experiences the working cycle composed of the off stage, the discharge stage, the self-excited discharge stage, and again the off stage. The air-gap presents different discharge characteristics in different stages [19]. We establish the air-gap model, taking Spark Plug_1 in Figure 2 as an example, in this paper.

The nodal voltages of 1, 2, 3, and 4 are denoted by u_1, u_2, u_3, and u_4, respectively; i_1, i_2, i_3, i_4, i_5, i_6, and i_7 represent the branch currents, respectively; i_g is the current through the spark plug air-gap; and u_g is the voltage of the spark plug.

a) There is no initial energy stored until the control signal is triggered ($t = t_1$). The primary winding then connects with the power supply and C_5 is charged. Because the spark plug voltage does not reach the breakdown voltage, it is in the off stage. In this stage, we can neglect the primary winding parasitic capacitances. Figure 4 shows the circuit model transformed to the s-domain.

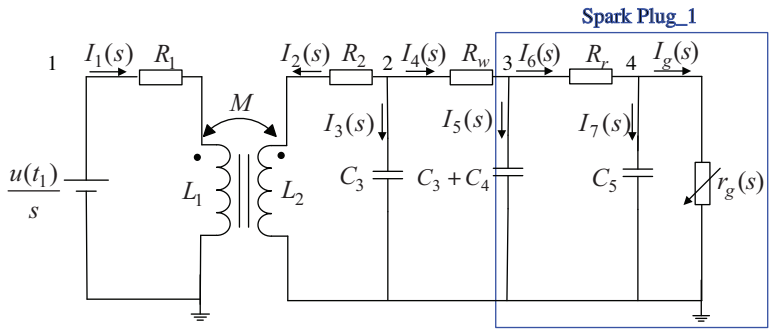

Figure 4. The circuit model when the spark plug is in the off stage $(t_1 < t < t_2)$.

The circuit model is governed by Kirchhoff's laws, and therefore it can be formulated in terms of nodal voltages and branch currents.

$$\begin{cases} \frac{u(t_1)}{s} = R_1 I_1(s) + sL_1 I_1(s) + sMI_2(s) \\ U_2(s) = R_2 I_2(s) + sL_2 I_2(s) + sMI_1(s) \\ I_2(s) + U_2(s)sC_3 + \frac{[U_2(s)-U_3(s)]}{R_w} = 0 \\ \frac{[U_2(s)-U_3(s)]}{R_w} = U_3(s)s(C_3+C_4) + \frac{[U_3(s)-U_4(s)]}{R_r} \\ \frac{[U_3(s)-U_4(s)]}{R_r} = U_4(s)(sC_5 + \frac{1}{r_g(s)}) \end{cases} \tag{7}$$

Solving Eq. (7) based on the condition of $r_g(s) = \infty$, we can obtain the primary winding current and the spark plug voltage:

$$\begin{cases} I_1(s) = \frac{1}{R_1+sL_1}\frac{u(t_1)}{s} + \frac{sM}{R_1+sL_1}(sC_3 + \frac{1}{R_w})U_2(s) - \frac{sM}{R_w(R_1+sL_1)}U_3(s) \\ U_g(s) = U_4(s) \end{cases} . \tag{8}$$

b) As soon as the control signal is cut off $(t = t_2)$, the primary current discharges through parasitic capacitance C_1, as shown in Figure 5. At the same time, C_5 is charged by the secondary current, which causes C_5's voltage to increase greatly and rapidly. The corona is therefore created between the 2 electrodes.

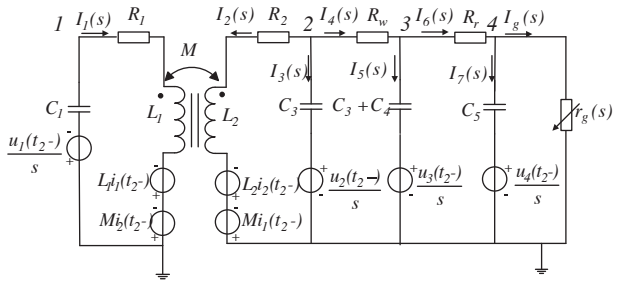

Figure 5. The circuit model when the spark plug is in the discharge stage $(t_2 \le t < t_3)$.

The circuit equations of nodal voltages and branch currents are controlled by:

$$\begin{cases} R_1 I_1(s) + sL_1 I_1(s) + \frac{1}{sC_1} I_1(s) + sMI_2(s) = L_1 i_1(t_2-) + Mi_2(t_2-) + \frac{u_1(t_2-)}{s} \\ U_2(s) = R_2 I_2(s) + sL_2 I_2(s) + sMI_1(s) - L_2 i_2(t_2-) - Mi_1(t_2-) \\ I_2(s) + [U_2(s) - \frac{u_2(t_2-)}{s}] sC_3 + \frac{[U_2(s)-U_3(s)]}{R_w} = 0 \\ \frac{[U_2(s)-U_3(s)]}{R_w} = [U_3(s) - \frac{u_3(t_2-)}{s}] s(C_3 + C_4) + \frac{[U_3(s)-U_4(s)]}{R_r} \\ U_g(s) = U_4(s) \end{cases} . \quad (9)$$

At this moment $(t = t_2)$, the parameters in the circuit model satisfy the following relations:

$$\begin{cases} r_g(s) = \infty \\ sI_1(s) >> sI_2(s) \\ L > M \end{cases} . \quad (10)$$

Under the conditions of Eq. (10), Eq. (9) can be simplified. The primary winding current and the spark plug voltage can then be expressed as:

$$\begin{cases} I_1(s) = [L_1 i_1(t_2-) + Mi_2(t_2-)] \frac{1}{R_1 + sL_1 + \frac{1}{sC_1}} \\ U_g(s) = U_4(s) \end{cases} . \quad (11)$$

When $t = t_2$, $u_4(t)$ reaches breakdown voltage V_{br}. The corona discharges and the spark plug breaks down. Therefore, positive and negative ions exist, and the resistance changes over time until the plasma is present $(t = t_3)$.

During this period $(t_2 \sim t_3)$, the primary winding current can be obtained by solving Eq. (9):

$$I_1(s) = \frac{1}{sM}[L_2 i_2(t_2-) + Mi_1(t_2-) - (R_2 + sL_2) C_3 u_2(t_2-)] + \frac{1}{sM}[(R_2 + sL_2)(\frac{1}{R_w} + sC_3) + 1] U_2(s) - \frac{R_2 + sL_2}{sMR_w} U_3(s). \quad (12)$$

During the process, the spark plug air-gap resistance can be computed by the Rompe-Weizel formula in the time domain [20]:

$$r_g(t) = l_g \left\{ \left(2\alpha / p \int_{t_1}^{t_2} i_g^2(t) dt \right) \right\}^{-0.5}, \quad (13)$$

where l_g is the length of the air-gap of the spark plug, α is the spark coefficient, and p is the pressure.

Since $r_g(t) << R_r$ and $i_6 << i_g$, the spark plug voltage and current have the following relations:

$$\begin{cases} i_g(t) + C_5 u_g'(t) = 0 \\ u_g(t) = i_g(t) r_g(t) \end{cases} . \quad (14)$$

The initial conditions at t_2 can be written as:

$$\begin{cases} u_g(t_2) \cong V_{br} \\ i_g(t_2) \cong 0 \end{cases} . \quad (15)$$

When substituting $i_g(t)$ from Eq. (13) into Eq. (14), the relations in Eq. (14) can be restated as:

$$\begin{cases} i_g(t) = K_1 u_g'(t) \\ i_g(t) = 2K_2^2 \left(\frac{i_g'(t)u_g^2(t) - i_g(t)u_g(t)u_g'(t)}{u_g^4(t)}\right) \end{cases}, \tag{16}$$

where $K_1 = -C_5$ and $K_2^2 = l_g^2 p/2\alpha$.

Eq. (18) can be restated as:

$$K_1 u_g'(t) = 2K_2^2 K_1 \left(\frac{u_g''(t)u_g^2(t) - u_g'(t)u_g(t)u_g'(t)}{u_g^4(t)}\right). \tag{17}$$

After solving Eq. (17) under the conditions of Eq. (15), the spark plug current and voltage can be written as:

$$\begin{cases} i_g(t) = 2\left|K_2 K_3\right| K_1 K_3^2 e^{2K_3^2 t + P_1} \left(1 + e^{2K_3^2 t + P_1}\right)^{-1.5} \\ u_3(t) = u_g(t) = 2\left|K_2 K_3\right| \left(1 + e^{2K_3^2 t + P_1}\right)^{-0.5} \end{cases}, \tag{18}$$

where $K_3 = V_{br}/2K_2$ and P_1 is an integral constant.

c) Once the plasma appears in the air-gap ($t = t_3$), the spark plug enters the self-excited discharge stage immediately. This period lasts until the spark current becomes smaller than the arc current ($t = t_4$).

The voltage of the spark plug remains constant during this phase ($t_3 \le t < t_4$), supposing in this paper that $u_g(t) = u_4(t) = U_0$ [21,22]. The circuit model is shown in Figure 6.

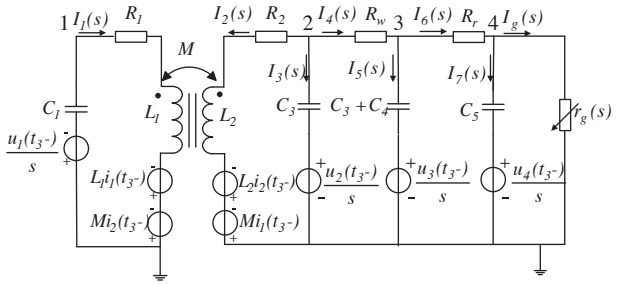

Figure 6. The circuit mode when the spark plug is in the self-excited discharge stage ($t_3 \le t < t_4$).

Nodal analysis is applied to obtain the circuit equations below.

$$\begin{cases} R_1 I_1(s) + sL_1 I_1(s) + \frac{1}{sC_1} I_1(s) + sMI_2(s) = L_1 i_1(t_3-) + Mi_2(t_3-) + \frac{u_1(t_3-)}{s} \\ U_2(s) = R_2 I_2(s) + sL_2 I_2(s) + sMI_1(s) - L_2 i_2(t_3-) - Mi_1(t_3-) \\ I_2(s) + [U_2(s) - \frac{u_2(t_3-)}{s}] sC_3 + \frac{[U_2(s) - U_3(s)]}{R_w} = 0 \\ \frac{[U_2(s) - U_3(s)]}{R_w} = [U_3(s) - \frac{u_3(t_3-)}{s}] s(C_3 + C_4) + \frac{[U_3(s) - U_4(s)]}{R_r} \\ U_4(s) = \frac{U_0}{s} \\ U_g(s) = U_4(s) \end{cases} \tag{19}$$

The primary winding current, the spark plug current, and the spark plug voltage can therefore be obtained.

$$\begin{cases} I_1(s) = \frac{1}{sM}[L_2 i_2(t_3-) + M i_1(t_3-) - (R_2+sL_2)C_3 u_2(t_3-)] + \frac{1}{sM}[(R_2+sL_2)(\frac{1}{R_w}+sC_3)+1]U_2(s) \\ \qquad -\frac{R_2+sL_2}{sMR_w}U_3(s) \\ I_g(s) = \frac{[U_3(s)-U_4(s)]}{R_r} - [U_4(s) - \frac{u_4(t_3-)}{s}]sC_5 \\ U_g(s) = \frac{U_0}{s} \end{cases} \tag{20}$$

d) As soon as the spark current becomes smaller than the arc current, the plasma diminishes and the spark plug returns to the off stage [23]. During this stage ($t_4 \le t < t_5$), the circuit model is as shown in Figure 7.

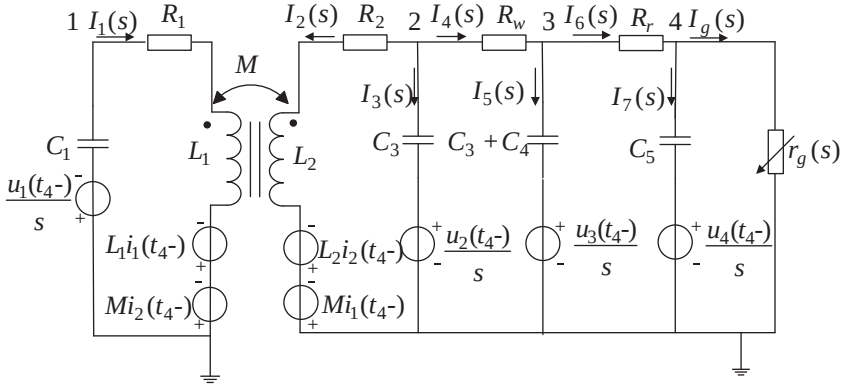

Figure 7. The circuit model during the stage in which the spark plug returns to the off stage ($t_4 \le t < t_5$).

Applying the nodal analysis, we have:

$$\begin{cases} R_1 I_1(s) + sL_1 I_1(s) + \frac{1}{sC_1}I_1(s) + sMI_2(s) = L_1 i_1(t_4-) + M i_2(t_4-) + \frac{u_1(t_4-)}{s} \\ U_2(s) = R_2 I_2(s) + sL_2 I_2(s) + sMI_1(s) - L_2 i_2(t_4-) - M i_1(t_4-) \\ I_2(s) + [U_2(s) - \frac{u_2(t_4-)}{s}]sC_3 + \frac{[U_2(s)-U_3(s)]}{R_w} = 0 \\ \frac{[U_2(s)-U_3(s)]}{R_w} = [U_3(s) - \frac{u_3(t_4-)}{s}]s(C_3+C_4) + \frac{[U_3(s)-U_4(s)]}{R_r} \\ \frac{[U_3(s)-U_4(s)]}{R_r} = [U_4(s) - \frac{u_4(t_4-)}{s}]sC_5 + \frac{U_4(s)}{r_g(s)} \\ U_g(s) = U_4(s) \end{cases} . \tag{21}$$

Solving Eq. (21) under the condition of $r_g(s) = \infty$, the primary winding current and the spark plug voltage can be obtained.

$$\begin{cases} I_1(s) = \frac{1}{sM}[L_2 i_2(t_4-) + M i_1(t_4-) - (R_2+sL_2)C_3 u_2(t_4-)] + \frac{1}{sM}[(R_2+sL_2)(\frac{1}{R_w}+sC_3)+1]U_2(s) \\ \qquad -\frac{R_2+sL_2}{sMR_w}U_3(s) \\ [1ex]U_g(s) = U_4(s) \end{cases} \tag{22}$$

The air-gap model of the spark plug is established based on the above analysis. After solving Eqs. (7)-(12) and Eqs. (18)-(22) and then taking the inverse Laplace transform, the current of the primary winding and the voltage of the spark plug during the working cycle can be obtained in the time domain.

4. Measurement and simulation

4.1. Parasitic parameters of the spark plug

According to the physical placement and the material characteristics of the spark plug, we extracted the parasitic parameters using the FEM approach: $C_q = 5.3986$ pF, $C_r = 5.8701$ pF, and $C_p = 4.9849$ pF. In order to confirm the parameters and the circuit model shown in Figure 2, the spark plug impedance characteristics were measured and simulated. The results are presented in Figure 8.

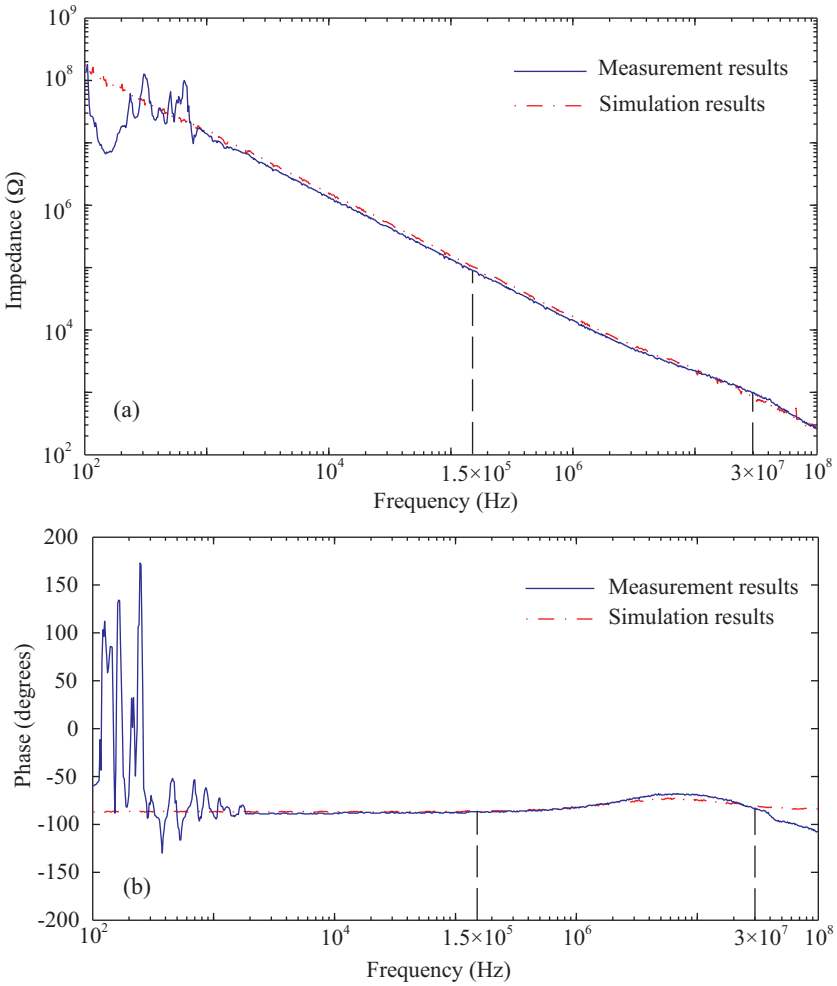

Figure 8. The spark plug impedance characteristics: a) amplitude-frequency characteristic, (b) phase-frequency characteristic.

Figure 8 shows the simulation results and measurement results of the spark plug impedance characteristics between the frequencies of 100 Hz and 100 MHz. It is shown that the simulation results are consistent with the measurement results within the frequencies between 150 kHz and 30 MHz. Therefore, the simulation results can reflect the impedance characteristics of the spark plug in the frequency band, and the parasitic capacitances values are verified for use in the circuit model in dealing with the conducted EMI problem. On the other hand, the measurement results are inconsistent with the simulation results in the range of frequency from 100 Hz to

2 kHz. This is mainly due to the test errors inherent in the measurement system. However, these errors have no significant impact on the analysis of the conducted EMI problem.

4.2. The circuit model of the spark plug in the ignition system

The simulated circuit model of the spark plug in the ignition system is shown in Figure 2. The parameters are: $U_s(t) = 12[\varepsilon(t-t_1) - \varepsilon(t-t_2)]$ V, $t_1 = 1.8$ ms, $t_2 = 3.2$ ms, $R_1 = 2\ \Omega$, $C_1 = 1.0\ \mu$F, $L_1 = 2.5$ mH, $L_2 = 5.6$ H, $M = 0.1$ H, $R_2 = 20\ \Omega$, $R_w = 2.8\ \mathrm{k}\Omega$, $C_3 = 1.5$ pF, $C_4 = 8.33$ pF, $C_5 = 7.92$ pF, $R_r = 4.98\ \mathrm{k}\Omega$, $V_{br} = 4.6$ kV, $U_0 = 350$ V, $l_g = 0.89$ mm, $p = 1$ atm, $\alpha = 1.1$ atm cm^2/(V^2 s), and $I_{sc} = 0.0015$ mA.

This experiment was carried out in a semianechoic chamber and the measurement system is shown in Figure 9. The ignition system of the automotive gasoline engine generator is supplied by a 12-V DC power supply via a line impedance stabilization network (LISN). The experimental system is located on the test platform on the ground. The measurement system comprises a digital oscilloscope (Tektronix DPO4104), a high-voltage probe (Tektronix P6015A), and a current probe (Tektronix A622). The measurement system for the current of the primary winding, the spark plug voltage at point A, and the LISN voltage at point B are given in Figure 9.

Figures 10 and 11 present the primary current and the spark plug voltage at point A, respectively, in the time domain, which were obtained by measurement and simulation.

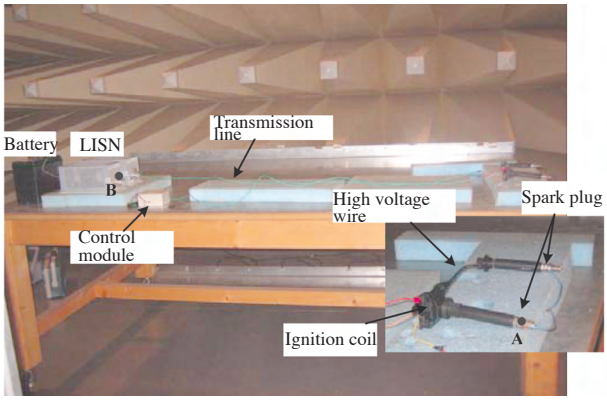

Figure 9. The experimental measurement system in a semianechoic chamber.

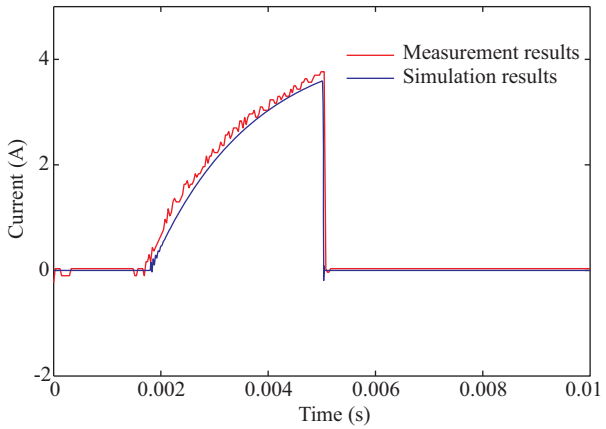

Figure 10. The simulated and measured current of the primary winding.

As shown in Figures 10 and 11, the simulated waveform is in good agreement with the measured waveform at various time points when the ignition system is working. Although there are some differences in amplitude, the measurements and simulations have the same trend in the time domain. This outcome demonstrates that the spark plug circuit model is correct.

4.3. Conducted EMI of the ignition system

According to the EMC measurement standards, the conducted EMI measurements were performed by observing the voltage developed across the defined LISN impedance [24]. The measurement results of the LISN voltage at point B in Figure 9 are shown in Figure 12.

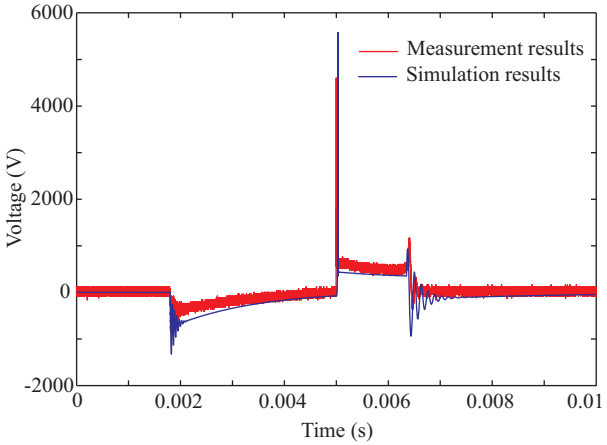

Figure 11. The simulated and measured voltage of the spark plug.

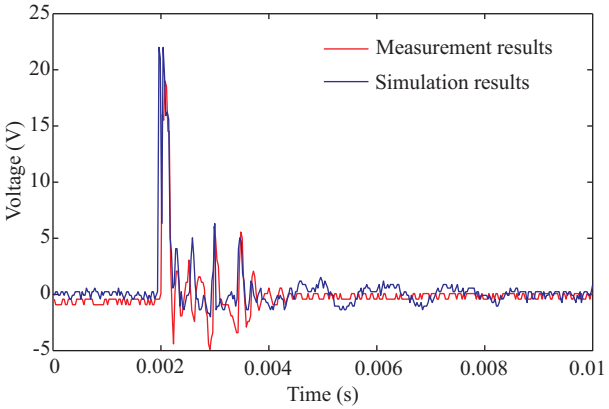

Figure 12. Measurement and simulation results of the LISN voltage.

The measured waveform is nearly the same as the simulated waveform in Figure 12. The results illustrate that the spark plug discharge is the main source of conducted EMI in the ignition system based on simulation.

5. Conclusion

This paper proposed a circuit model for analysis of the spark plug's conducted EMI in the ignition system. The circuit model emphasized the parasitic capacitances and the air-gap characteristics of the spark plug. The model was established after analyzing the spark plug's internal discharge channel. The approach for extraction of the spark plug parasitic parameters was discussed within the context of the FEM. The spark plug impedance characteristic simulation results coincided with the measurements, especially in the frequency band between 150 kHz and 30 MHz. The discharge processes and mechanisms of different spark plug stages were described in detail in this paper, using the electric circuit principles and the air-discharge theory. The primary current and the spark plug voltage simulations showed an exciting consistency with the measurements, which validated the effectiveness of the model. The ignition system's conducted EMI was simulated with the proposed model and the results confirmed that the spark plug discharge was the main source of the conducted EMI in the ignition system.

With rising constraints on energy resources and increasing concerns about the environment, the consumer as well as the automotive industry will pay more attention to conducted EMI. As a result, modeling and simulation will play important roles in automotive design and development. The modeling method described in this paper is indeed useful for the analysis of automotive conducted EMI.

Acknowledgment

This work was partially supported by the National Natural Science Foundation of China (No. 50877081) and partially supported by the Third Stage Training of the "211 Project" of Chongqing University (S-09111).

References

[1] G.P. Liu, Anticipating System-Level Electromagnetic Interference Using Numerical Methods and Measurement Techniques, PhD dissertation, Department of Electrical Engineering, University of Missouri - Rolla, USA, 2004.

[2] C. Chen, "Predicting vehicle-level EMC performance utilizing on-bench component characterization results", IEEE International Symposium on Electromagnetic Compatibility, Vol. 2, pp. 765-769, 1999.

[3] R.R. Burgett, R.E. Massoll, B.R. Van Uum, "Relationship between spark plugs and engine-radiated electromagnetic interference", IEEE Transactions on Electromagnetic Compatibility, Vol. 3, pp. 160-172, 1974.

[4] International Electrotechnical Commission, CISPR 25: Radio Disturbance Characteristics for the Protection of Receivers Used on Board Vehicles, Boats and on Devices - Limits and Methods of Measurement, Geneva, IEC, 2008.

[5] G. Apaydın, N. Arı, "EMC education at the University of Technology Zurich", Turkish Journal of Electrical Engineering & Computer Sciences, Vol. 17, pp. 261-272, 2009.

[6] S. Frei, R.G. Jobava, D. Topchishvili, "Complex approaches for the calculation of EMC problems of large systems", IEEE International Symposium on Electromagnetic Compatibility, Vol. 3, pp. 826-831, 2004.

[7] R.G. Jobava, F.G. Bogdanov, A.L. Gheonjian, S. Frei, "Analysis of influence of vehicle bodyshell on the characteristics of wire antennas using a new MoM-based EM/EMC solver", IEEE International Symposium on Antennas and Propagation, Vol. 4, pp. 831-834, 2003.

[8] G. Anzaldi, P.J. Riu, F. Silva, R. Santos, "Finite difference time domain low cost modeling for automotive environments", IEEE International Symposium on Electromagnetic Compatibility, Vol. 3, pp. 775-780, 2004.

[9] D.D. Ward, S. Lawton, "Numerical modelling for automotive EMC", IEEE International Symposium on Electromagnetic Compatibility, pp. 222-227, 1995.

[10] L. Štrac, F. Kelemen, D. Žarko, "Modeling and calculation of electromagnetic field in the surroundings of a large power transformer", Turkish Journal of Electrical Engineering & Computer Sciences, Vol. 17, pp. 301-314, 2009.

[11] G. Çakir, M. Çakir, L. Sevgi, "Electromagnetic radiation from multilayer printed circuit boards: a 3D FDTD-based virtual emission predictor", Turkish Journal of Electrical Engineering & Computer Sciences, Vol. 17, pp. 315-325, 2009.

[12] M.S. Mamiş, A. Kaygusuz, M. Köksal, "State variable distributed-parameter representation of transmission line for transient simulations", Turkish Journal of Electrical Engineering & Computer Sciences, Vol. 18, pp. 31-42, 2010.

[13] R.A. Shepherd, J.C. Gaddie, D.L. Nielson, "New techniques for suppression of automobile ignition noise", IEEE Transactions on Vehicular Technology, Vol. 25, pp. 2-12, 1976.

[14] F.A. Soldera, F.T. Mucklich, K. Hrastnik, T. Kaiser, "Description of the discharge process in spark plugs and its correlation with the electrode erosion patterns", IEEE Transactions on Vehicular Technology, Vol. 53, pp. 1257-1265, 2004.

[15] O. Fujiwara, Y. Amemiya, "Calculation of ignition noise level caused by plug gap breakdown", IEEE Transactions on Electromagnetic Compatibility, Vol. 24, pp. 26-32, 1982.

[16] Q. Wang, Y. Zhao, S. Li, Z. Zhao, "Research on energy simulation model for vehicle ignition system", IEEE Vehicle Power and Propulsion Conference, pp. 1-5, 2008.

[17] J. Jia, Q. Wang, J. Yu, Y. Zheng, "Wideband equivalent circuit model and parameter computation of automotive ignition coil based on finite element analysis", Application Computational Electromagnetics Society Journal, Vol. 25, pp. 612-619, 2010.

[18] H. Qu, L. Kong, Y. Xu, X. Xu, Z. Ren, "Finite-element computation of sensitivities of interconnect parasitic capacitances to the process variation in VLSI", IEEE Transactions on Magnetics, Vol. 44, pp. 1386-1389, 2008.

[19] W. Guan, Automobile Structure, Beijing, China Machine Press, 2005, pp. 239-256 (in Chinese).

[20] T.G. Engel, A.L. Donaldson, M. Kristiansen, "The pulsed discharge arc resistance and its functional behavior", IEEE Transactions on Plasma Science, Vol. 17, pp. 323-329, 1989.

[21] K.J. Tseng, Y.M. Wang, D.M. Vilathgamuwa, "An experimentally verified hybrid Cassie-Mayr electric arc model for power electronics simulations", IEEE Transactions on Power Electronics, Vol. 12, pp. 429-436, 1997.

[22] G.C.R. Sincero, J. Cros, P. Viarouge, "Arc models for simulation of brush motor commutations", IEEE Transactions on Magnetics, Vol. 44, pp. 1518-1521, 2008.

[23] C.R. Paul, Introduction to Electromagnetic Compatibility, New York, Wiley, 1992, pp. 317-327.

[24] T. Williams, EMC for Product Designers, Wareham, the Netherlands, Elsevier, 2007, pp. 107-109.